Figure 4.15: $G_{even,data}(V,T)$ as a function of V at several temperatures.

$$G_{odd,data}(V,T) \equiv \frac{G_{remainder}(V,T) - G_{remainder}(-V,T)}{2}, \qquad (4.10)$$

respectively. According to the definitions (4.9) and (4.10), we plot $G_{even,data}(V,T)$ and $G_{odd,data}(V,T)$ in Fig. 4.15 and Fig. 4.16 respectively.
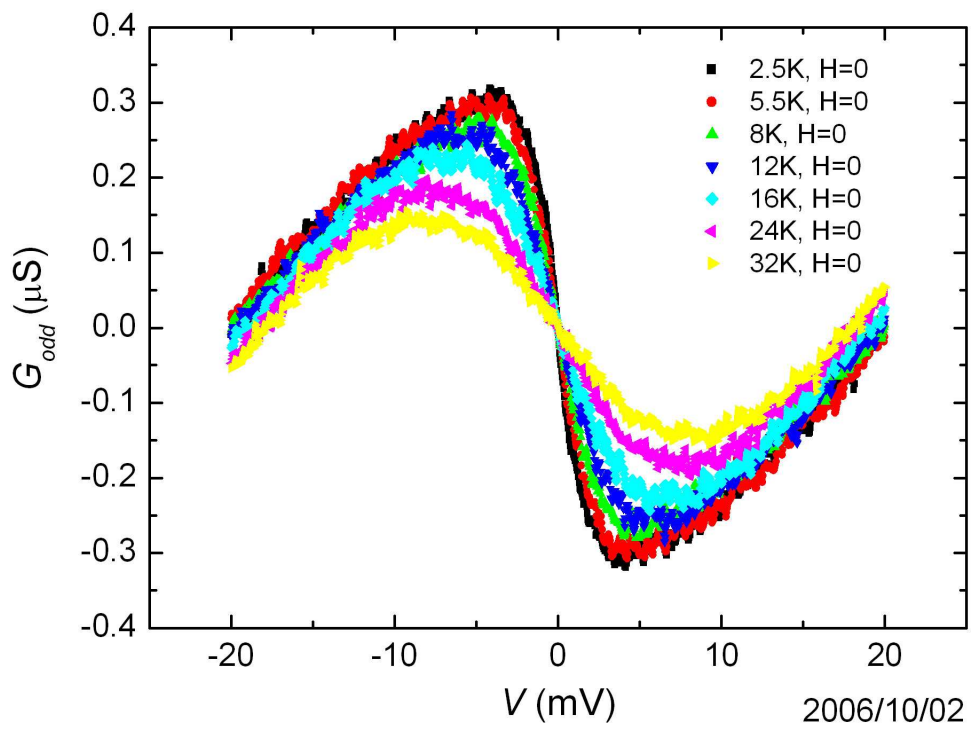
Figure 4.16: $G_{odd,data}(V, T)$ as a function of V at several temperatures.

4.5 Weak Coupling Regime

4.5.1 $G_{even,data}(V,T)$

Now, we want to fit the $G_{even,data}(V,T)$ using the theoretical calculation for the even conductance in the weak coupling regime, $G_{even,weak}(V,T)$. From (2.144), $G_{even,weak}(V,T)$ can be expressed as

$$G_{even}^{weak}(V,T) = A - B \int_{-\infty}^{\infty} [\int_{-E_0}^{E_0} \frac{\tanh(\frac{\epsilon'}{2k_B T})}{\epsilon' - \omega} d\epsilon'] \frac{\partial f(\omega - eV)}{\partial \omega} d\omega \tag{4.11}$$

$$\approx A - B \ln\frac{[(eV)^2 + (nk_B T)^2]^{1/2}}{E_0}, \tag{4.12}$$

where (4.12) is an interpolation function of (4.11) [39]. We will fit the data using the integration form (4.11) instead of the interpolation function (4.12).

There are three parameters in (4.11): A, B, and E_0. According to (4.12), the effect of E_0 is to result an offset, $-B \ln E_0$. It means that if B was fixed, the effect of varying E_0 is equivalent to the effect of varying A. Since the validity of (4.11) is based on the assumption that $eV << E_0$, we arbitrarily choose $E_0 = 100$ meV, which is much greater than the boundary of the region ($\sim \pm 20$ mV) within which the conductance peak occurs. After fixing the value of E_0, we have two parameters A and B to be fitted. The fitting procedures are described in the following: For a fixed temperature T_i, we plot the magnitudes of $G_{even,data}(V_i, T_i)$ v.s. the magnitudes of $h(V_i, T_i)$ for each V_i, where V_i is the voltage part of each data point $(V_i, G_{even,data}(V_i, T_i))$ in the $G_{even,data}(V,T)$ spectra, where

$$h(V,T) \equiv \int_{-\infty}^{\infty} [\int_{-E_0}^{E_0} \frac{\tanh(\frac{\epsilon'}{2k_B T})}{\epsilon' - \omega} d\epsilon'] \frac{\partial f(\omega - eV)}{\partial \omega} d\omega. \tag{4.13}$$

If $G_{even}^{weak}(V,T)$ can describe $G_{even,data}(V,T)$, the plot should be linear, i.e.,

$$G_{even,data}(V_i,T_i) = a(T_i) + b(T_i)\ h(V_i,T_i), \qquad (4.14)$$

and the parameters $A(T_i)$ and $B(T_i)$ are determined as

$$\begin{aligned} A(T_i) &= a(T_i), \\ B(T_i) &= -b(T_i). \end{aligned} \qquad (4.15)$$

We repeat the procedures mentioned above for all the T_i's at which we take the data. If the number of T_i's is N_T, after running over all the T_i's, we will get N_T "$G_{even,data}(V_i,T_i)$ v.s. $h(V_i,T_i)$" curves. According to Appelbaum's theory, A and B are constants to temperature, so all these N_T curves should collapse onto a single straight line.

Fig. 4.17 shows the $G_{even,data}(V_i,T_i)$ v.s. $h(V_i,T_i)$ relations for all the temperatures at which we measured the $G(V,T)$ spectra. Here $h(V,T)$ was calculated numerically using Simpson's rule, which is described in appendix B. We find, in Fig. 4.17, the $G_{even,data}(V_i,T_i)$ v.s. $h(V_i,T_i)$ relations are nearly linear for $T = 32$, 24, and 16 K, and deviate from the linearity for $T = 12$, 8, 5.5, and 2.5 K. The lower the temperature, the larger the deviation. We focus on the liner relation and determine the linear function. As shown in Fig. 4.18, for $T = 32$, 24, and 16 K, the fitted linear function is

$$G_{even,data}(V,T) = 0.95\ h(V,T) - 2.618, \qquad (4.16)$$

Therefore from (4.11), and (4.13)$\sim$(4.15), the A and B parameters in (4.11) can be determined as -2.618 and -0.95 respectively.
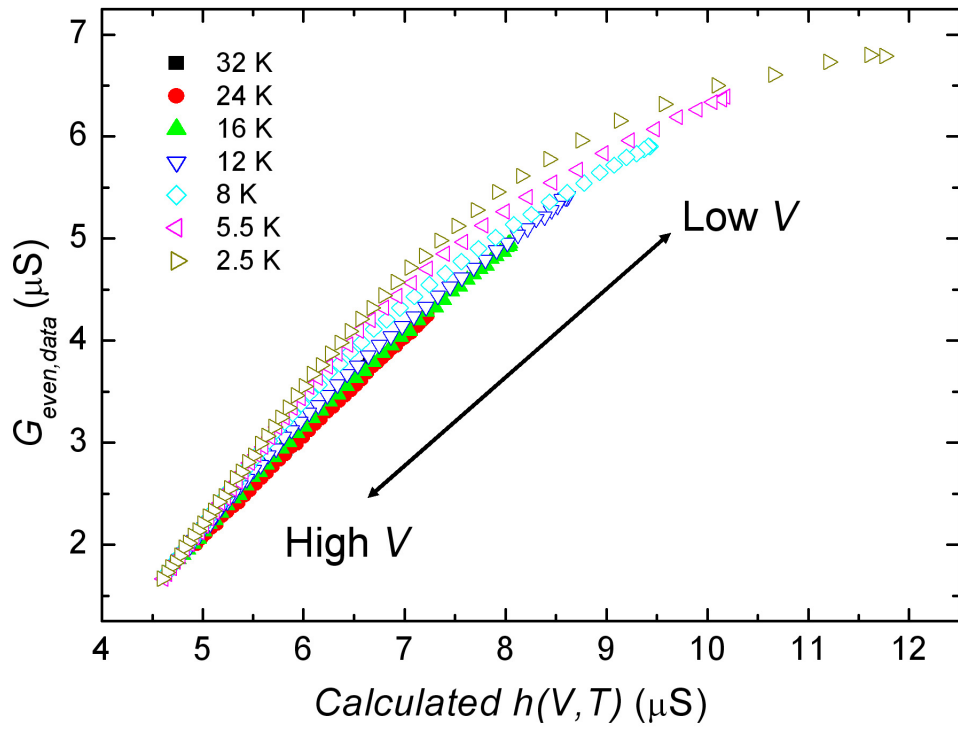
87

Figure 4.17: $G_{even,data}(V, T)$ vs. $h(V, T)$ plots at several temperatures.

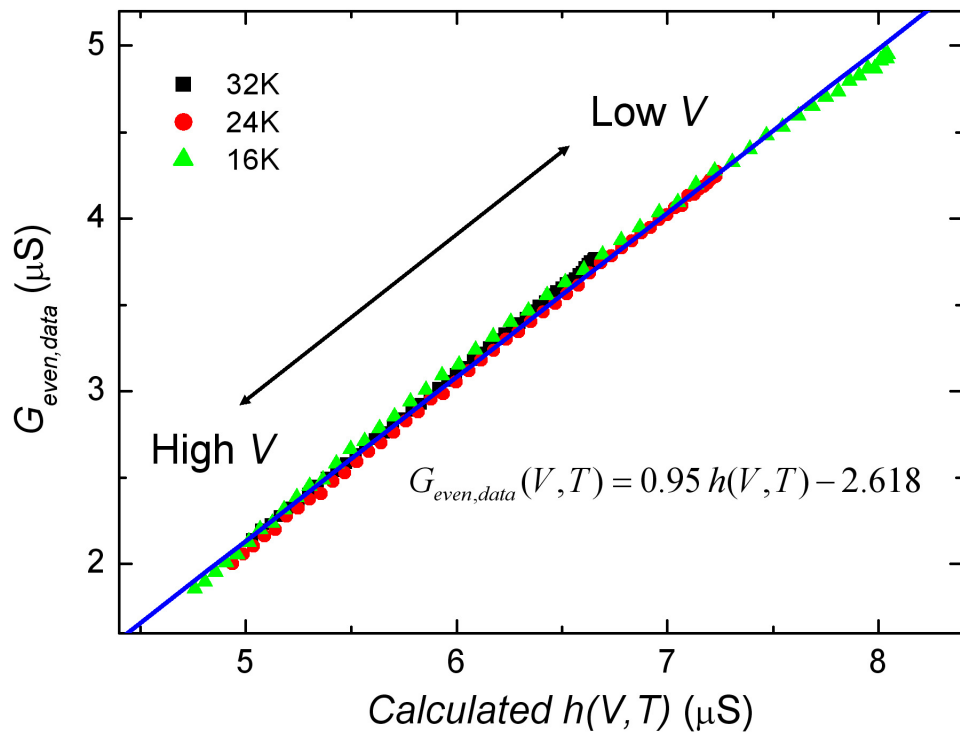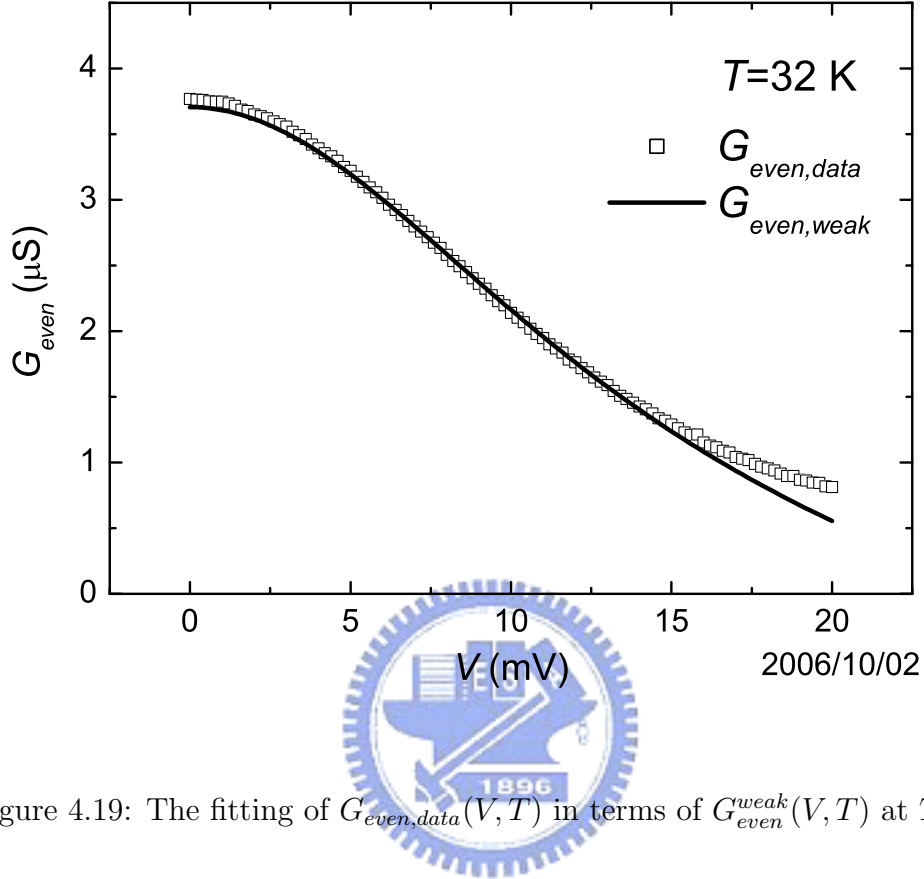Figure 4.18: The linear fitting of $G_{even,data}(V,T)$ vs. $h(V,T)$ plots at $T = 32, 24, 16$ K.

Figure 4.19: The fitting of $G_{even,data}(V,T)$ in terms of $G_{even}^{weak}(V,T)$ at $T = 32$ K.

Using these parameters values, we plot $G_{even}^{weak}(V,T)$ as a function of V for all the T_i's and compare these with $G_{even,data}(V_i, T_i)$. Fig. 4.19 $\sim$ Fig. 4.25 show the results for each T_i. We find for $T = 32$ K, 24 K, and 16 K, the theory can describe the data well, but the data deviate from the theoretical calculation for $T \lesssim 12$ K, the lower the temperature, the larger the deviations. This is consistent with the plots of $G_{even,data}(V_i, T_i)$ v.s. $h(V_i, T_i)$ as shown in Fig. 4.17. The results for $T = 32$, 24, and 16 K are combined in Fig. 4.26, and the results for $T = 12$, 8, 5.5, and 2.5 K are combined in Fig. 4.27.

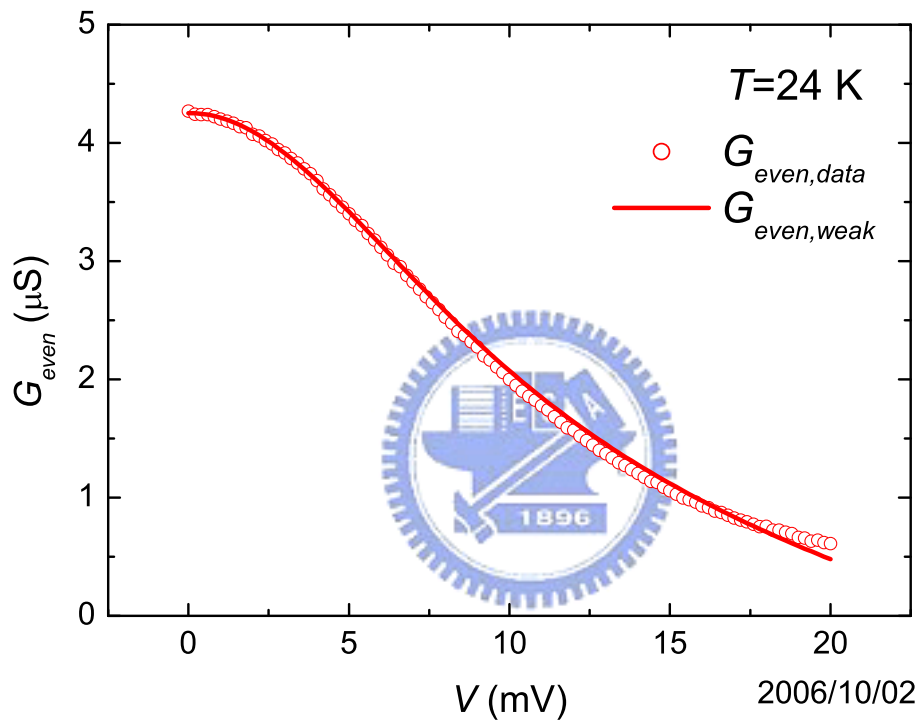The deviations of the theoretical curves from the data can be understood

90

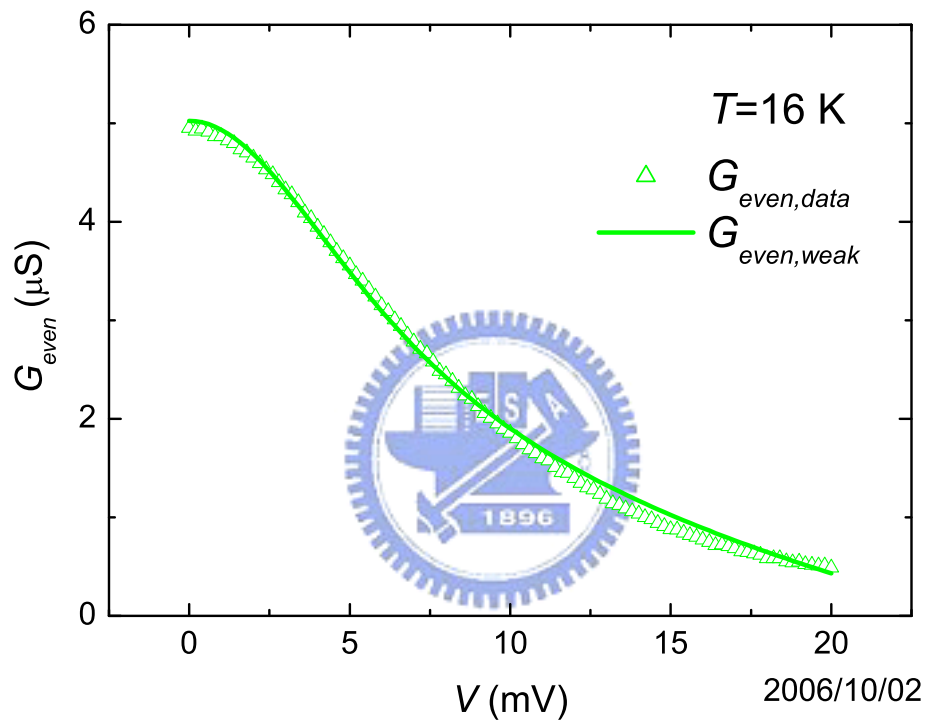Figure 4.20: The fitting of $G_{even,data}(V, T)$ in terms of $G_{even}^{weak}(V, T)$ at $T = 24$ K.

Figure 4.21: The fitting of $G_{even,data}(V,T)$ in terms of $G_{even}^{weak}(V,T)$ at $T = 16$ K.

Figure 4.22: The fitting of $G_{even,data}(V,T)$ in terms of $G_{even}^{weak}(V,T)$ at $T = 12$ K.

Figure 4.23: The fitting of $G_{even,data}(V,T)$ in terms of $G_{even}^{weak}(V,T)$ at $T = 8$ K.
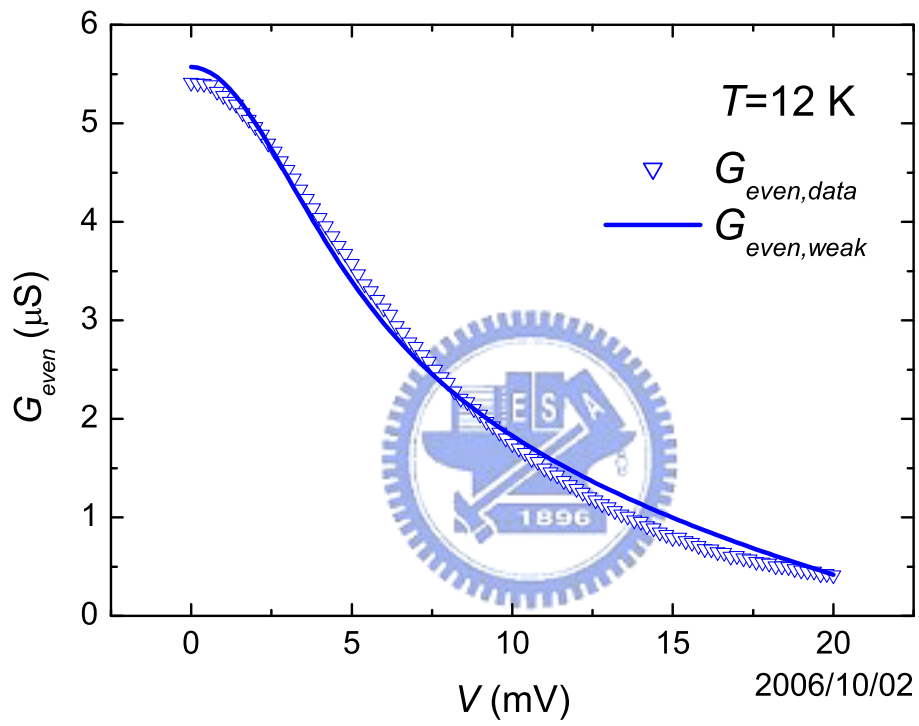
Figure 4.24: The fitting of $G_{even,data}(V,T)$ in terms of $G_{even}^{weak}(V,T)$ at $T = 5.5$ K.

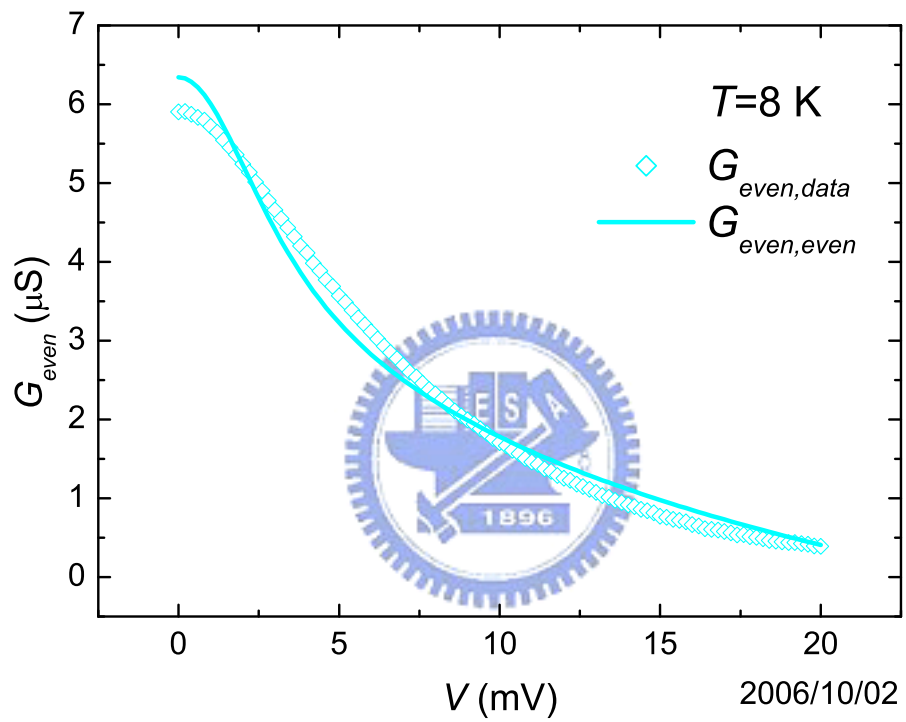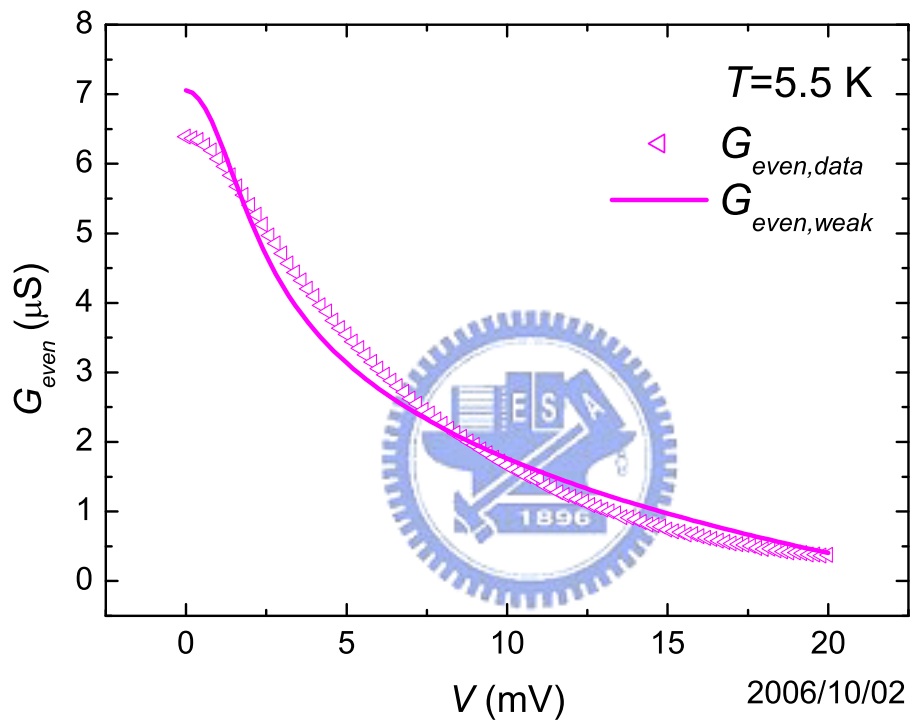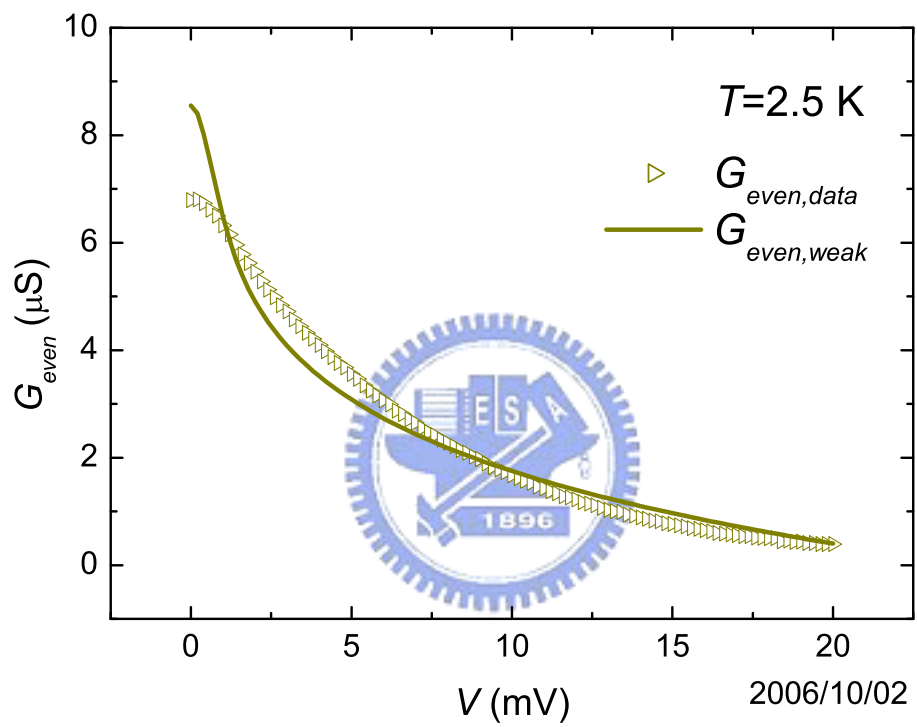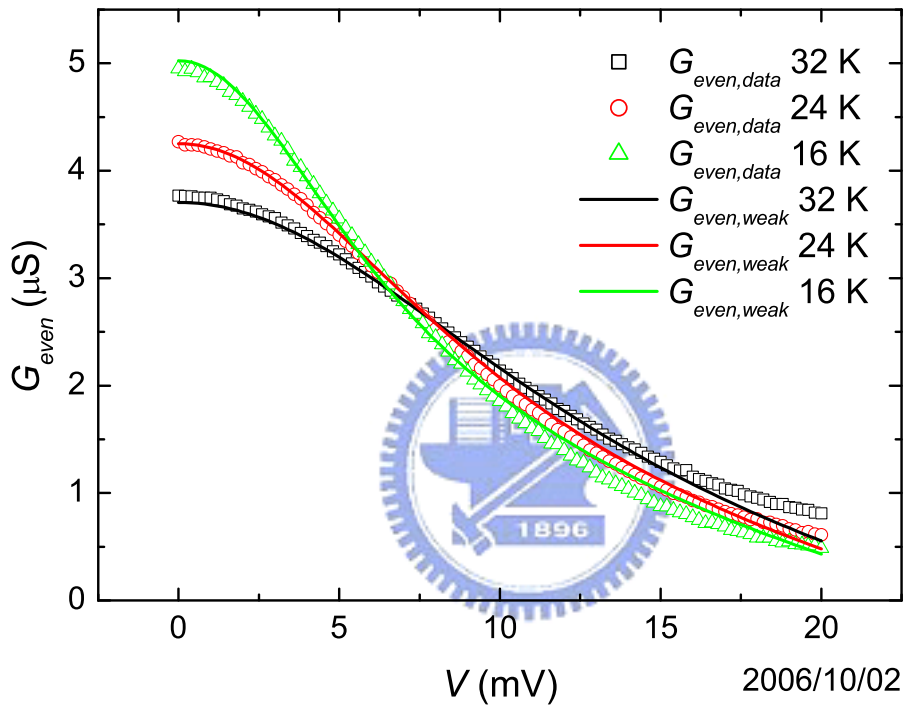Figure 4.25: The fitting of $G_{even,data}(V,T)$ in terms of $G_{even}^{weak}(V,T)$ at $T = 2.5$ K.

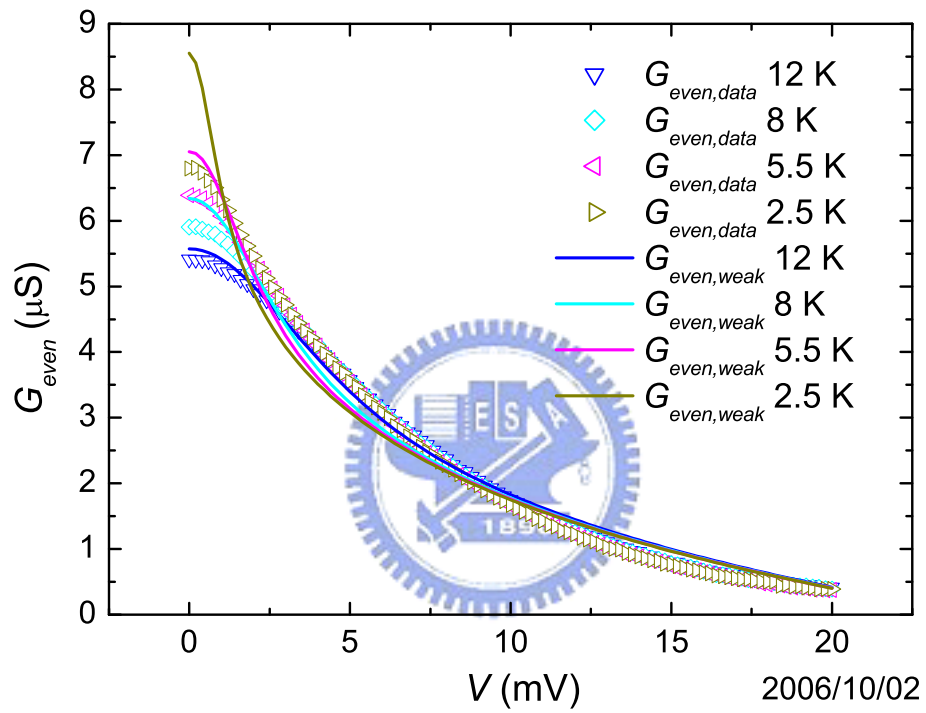Figure 4.26: The fitting of $G_{even,data}(V,T)$ in terms of $G_{even}^{weak}(V,T)$ at $T = 32$, 24, and 16 K.

Figure 4.27: The fitting of $G_{even,data}(V,T)$ in terms of $G_{even}^{weak}(V,T)$ at $T = 12, 8, 5.5$, and 2.5 K.

as the following: Appelbaum calculated the transition rate due to $s - d$ exchange interaction *perturbatively* to second order Born's approximation, and the using of perturbation method is valid if the coupling between the conduction electrons and localized spins is weak. In these $Al/AlO_x/Sc$ tunnel junctions, for $T \gtrsim 16$ K, the coupling is weak and therefore the theory can describe the data well. For $T \lesssim 12$ K, the singlet ground state gradually forms and the coupling gets stronger as the temperature goes lower, and therefore the data gradually depart from the theoretic curves, the lower the temperature, the more serious the departure.

4.5.2 $G_{even,data}(0, T)$

Now we turn to the zero-bias conductance as a function of temperature. We use the same values of E_0, A, and B mentioned above to calculate $G_{even}^{weak}(0, T)$ numerically. Fig. 4.28 shows the plots of both $G_{even,data}(0, T)$ and $G_{even}^{weak}(0, T)$ as functions of T. Here the $G_{even,data}(0, T)$ v.s. T is similar to the original measured $G(0, T)$ v.s. T as shown in Fig. 4.5. The difference between them is that in Fig. 4.5, $G(0, T)$ contains the contribution of the background at $V = 0$, but in Fig. 4.28, the background has been subtracted.

We find, in Fig. 4.28, the theoretically calculated zero-bias conductance, $G_{even,data}(0, T)$, has $-\log T$ dependence. For 14 K $\lesssim T \lesssim$ 32 K, the theoretical calculation can describe the data well, but for $T \lesssim 14$ K, the data start to deviate from the $-\log T$ dependence. The lower the temperature, the larger the deviation, which is consistent with the spectra fitting mentioned above. We should note $G_{even,data}(0, T)$ gradually saturates at low temperatures. Therefore, from the $G_{even,data}(0, T)$ fitting, we can roughly say 14 K $\lesssim T \lesssim$ 32 K is the weak coupling regime. In Fig. 4.28, we also

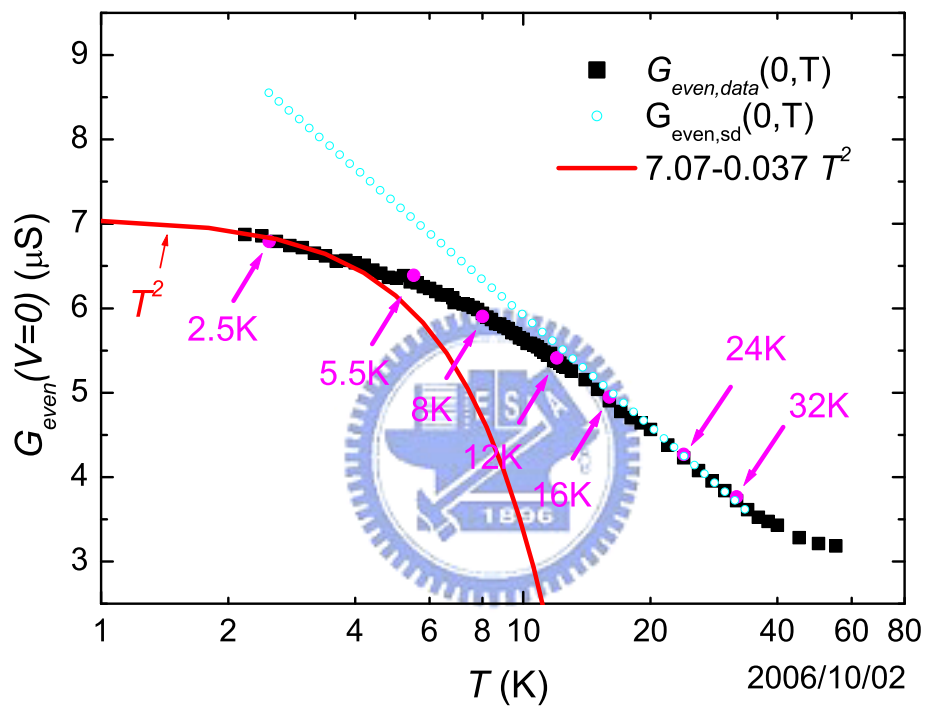Figure 4.28: The fitting of $G_{even,data}(0,T)$ in terms of $G_{even}^{weak}(0,T)$.

find at low temperatures ($T \lesssim 3.6$ K), $G_{even,data}(0,T)$ has "$c - dT^2$" behavior, which marks the strong coupling regime, and will be discussed latter.

4.5.3 $G_{odd,data}(V,T)$

After fitting $G_{even,data}(V,T)$ in terms of $G_{even}^{weak}(V,T)$, we turn to the asymmetric data, $G_{odd,data}(V,T)$. According to Appelbaum's theory described in chapter 2, in addition to the $s - d$ exchange interaction, the existence of the localized state in the insulating barrier will cause an assisted tunneling channel due to the impurity potential scattering. This channel will interfere with the the $s-d$ interaction channel and cause an symmetric tunneling current, and therefore, an asymmetric differential conductance. The asymmetric conductance, according to (2.146), is

$$
\begin{aligned}
G_{odd}^{weak}(V,T) &= \frac{6\pi^3 e^2 T_a T_J}{\hbar} \rho^b(0)\rho^a(0)(J\rho^a)^2 \int_{-\infty}^{\infty} d\omega \{ \frac{-\partial f(\omega + eV)}{\partial(eV)} \\
&\quad \times \tanh\frac{\omega}{2k_B T}(1 - 6J\rho^a \ln|\frac{\omega}{E_0}|) \} \\
&= \alpha \int_{-\infty}^{\infty} d\omega \frac{-\partial f(\omega + eV)}{\partial(eV)} \tanh\frac{\omega}{2k_B T}(1 - 6J\rho^a \ln|\frac{\omega}{E_0}|),
\end{aligned}
$$

(4.17)

where

$$
\alpha = \frac{6\pi^3 e^2 T_a T_J}{\hbar} \rho^b(0)\rho^a(0)(J\rho^a)^2.
$$

(4.18)

Note that $G_{odd}^{weak}(V,T)$ is asymmetric to V. And we should note in Appelbaum's derivations, the localized spins are assumed to be present in the vicinity of the (lead A)-(insulator) interface, and the bias V is applied to lead A while treating lead B as ground. A corresponds to the Sc lead, and B corresponds to the Al lead, in our Al/AlO$_x$/Sc case.

101

We think the asymmetric term in the data, $G_{odd,data}(V,T)$, may be due to the interference effect as described by Appelbaum, and try to fit it by $G_{odd}^{weak}(V,T)$. There are three parameters α, $J\rho^a$, and E_0 in $G_{odd}^{weak}(V,T)$, as shown in (4.17). We find just tuning these three parameters cannot fit the data except we add another parameter β to multiply $2k_BT$ in the denominator of hyperbolic tangent function. Since we set $E_0 = 100$ meV in the $G_{ven,data}(V,T)$ fitting, we adopt the same E_0 value and add another parameter γ to multiply E_0 in the denominator of the logarithmic function. Finally, we have totally four parameters, α, β, γ, and $J\rho^a$, and the formula in (4.17) can be written as

$$G_{odd}^{weak}(V,T) = \alpha \int_{-\infty}^{\infty} d\omega \frac{-\partial f(\omega + eV)}{\partial(eV)} \tanh \frac{\omega}{2k_BT\beta}(1 + 6J\rho^a\ln|\frac{\omega}{\gamma E_0}|). \qquad (4.19)$$

First, we fit $G_{odd,data}(V,T)$ by (4.19) at $T = 32$ K. The integration in (4.19) was carried out using Simpson's rule as in the case of $G_{even,data}(V,T)$ fitting. The result is plotted in Fig. 4.29 and the parameters values obtained from the fitting are $\alpha = -1.4$, $\beta = 5$, $\gamma = 0.0348$, and $J\rho^a = 0.1$. Here $J\rho^a > 0$ represents antiferromagnetic coupling between the conduction electrons and the localized spins ($J > 0$). We should note that the fitted $\alpha < 0$ is contradicts the definition in (4.18) which guarantees $\alpha > 0$. This is because in our measurement, we apply the bias V to the Sc lead and treating the Al lead as ground as mentioned in chapter 3. But to derive (4.19), Appelbaum assumed the bias V was applied to the lead which is closer to the localized spins. If we change the electrical polarity in our measurement, i.e., apply bias V to the Al lead while treating Sc lead as ground, then we will get $\alpha = +1.4 > 0$, which is consistent with the definition in (4.18). This seems implying that the localized spins (the diffused Sc atoms) in the insulating barrier are closer to the Al lead than to the Sc lead although this violates our intuition that the localized

102

spins (Sc atoms) are closer to the Sc lead since they should diffuse from the Sc lead into the insulating barrier.

Let us temporarily put aside the violation of the intuition and return to Fig. 4.29 again. The theoretical calculation $G_{odd}^{weak}(V,T)$ describe the data $G_{odd,data}(V,T)$ quite well at $T = 32$ K. We then use the same parameters values to plot the theoretical calculation at other temperatures as we had done in the $G_{even,data}(V,T)$ fitting. We find, at $T = 24$ K, the deviation between $G_{odd}^{weak}(V,T)$ and $G_{odd,data}(V,T)$ appears, which can be seen in Fig. 4.30. In Fig. 4.29 $\sim$ Fig. 4.37, we find the lower the temperature, the larger the deviation.

4.6　Strong Coupling Regime

For 16 K $\lesssim T \lesssim$ 32 K, Appelbaum's perturbation calculation can describe both $G_{even,data}(V,T)$ as a function of V and the $-\log T$ dependence of $G_{even,data}(0,T)$ well. But the data deviate from the theoretical prediction as $T \lesssim$ 16 K, and gradually saturate at low temperatures ($\sim$ 2.5 K). This is due to as $T < T_K$, the perturbation method breaks down as mentioned in chapter 2. When $T \to 0$, the system will reach its singlet ground state and can be described by the Fermi liquid theory. In this low temperature limit regime, the zero-bias conductance has $c - dT^2$ dependence as shown in Fig. 4.28. The $G(0,T)$ can be calculated by the Numerical Renormalization Group (NRG) method [13, 33] for the whole temperature regime. Goldhaber-Gordon [21] found an empirical expression which can well approximate the result of the numerical calculation, as mentioned in (2.82) (in the tunnel junction
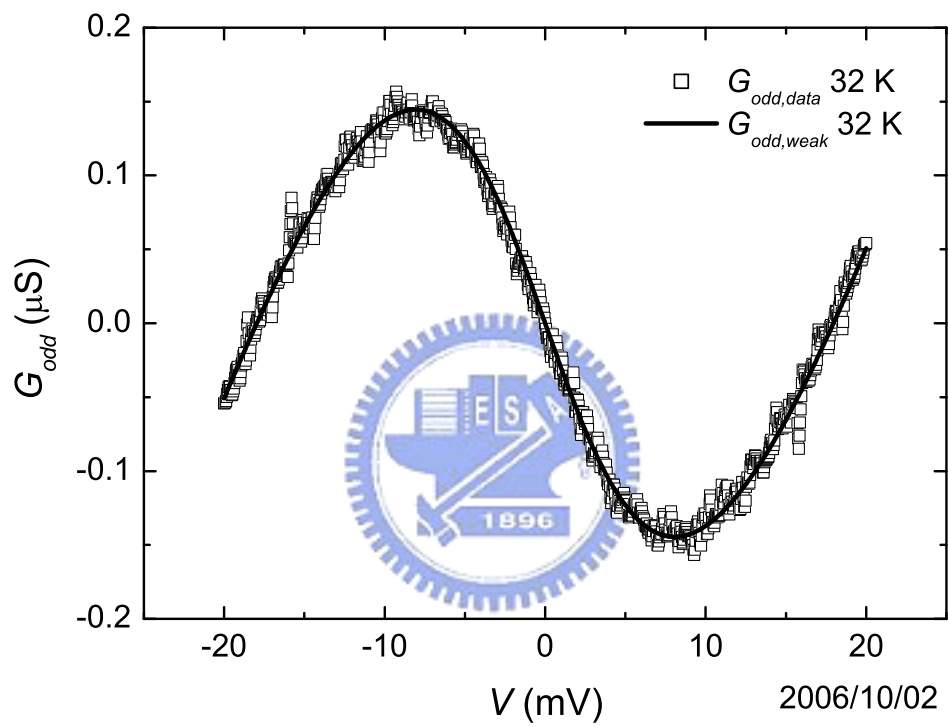
103

Figure 4.29: The fitting of $G_{odd,data}(V,T)$ in terms of $G_{odd}^{weak}(V,T)$ at $T = 32$ K.
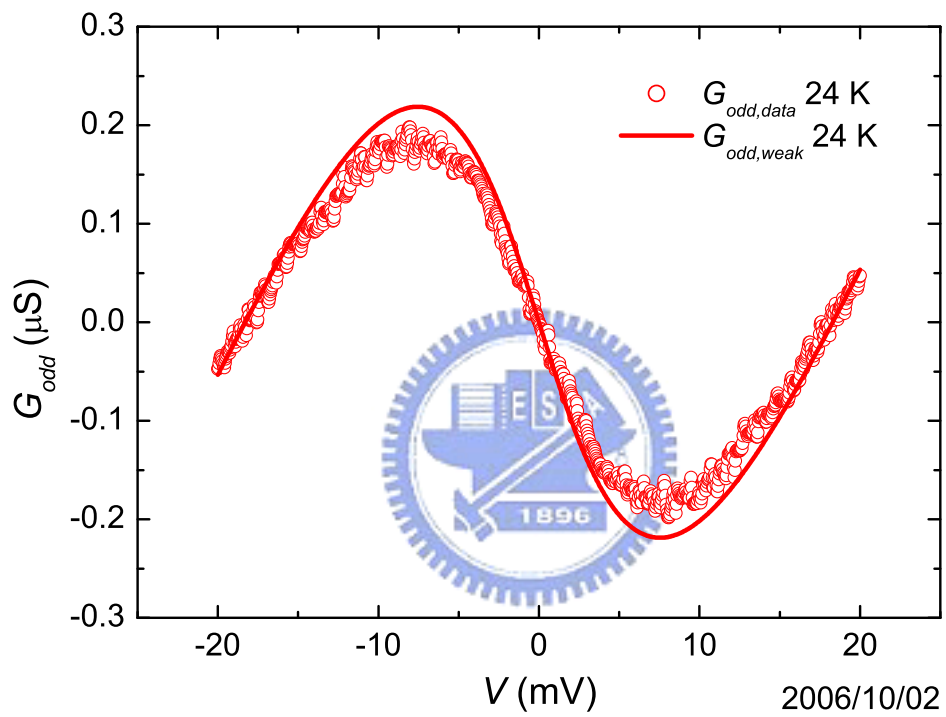
Figure 4.30: The fitting of $G_{odd,data}(V,T)$ in terms of $G_{odd}^{weak}(V,T)$ at $T = 24$ K.

Figure 4.31: The fitting of $G_{odd,data}(V,T)$ in terms of $G_{odd}^{weak}(V,T)$ at $T = 16$ K.

Figure 4.32: The fitting of $G_{odd,data}(V,T)$ in terms of $G_{odd}^{weak}(V,T)$ at $T = 12$ K.

Figure 4.33: The fitting of $G_{odd,data}(V,T)$ in terms of $G_{odd}^{weak}(V,T)$ at $T = 8$ K.

Figure 4.34: The fitting of $G_{odd,data}(V, T)$ in terms of $G_{odd}^{weak}(V, T)$ at $T = 5.5$ K.

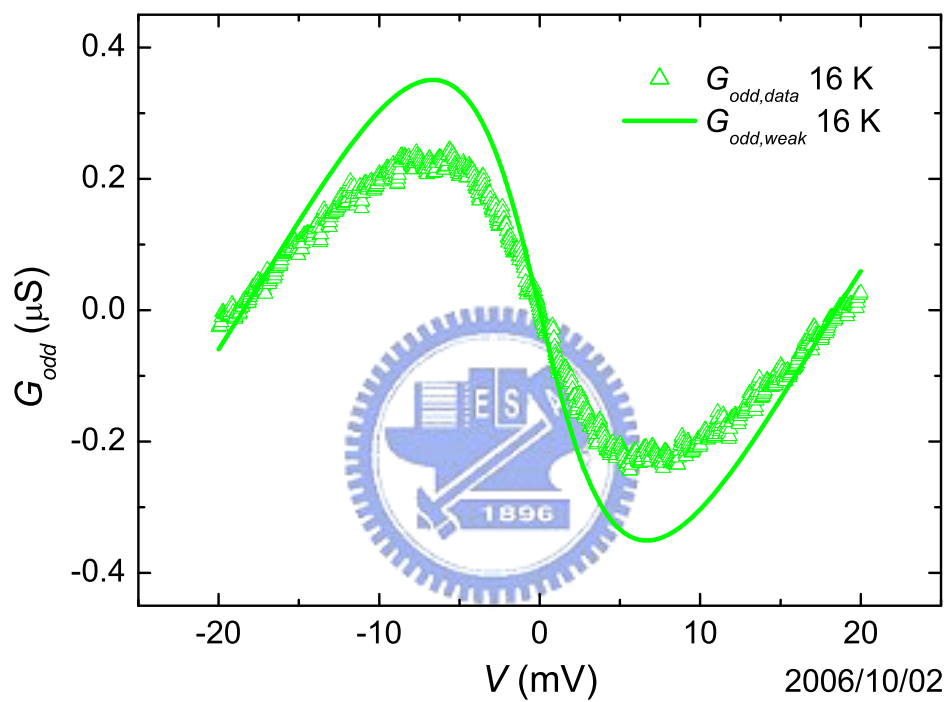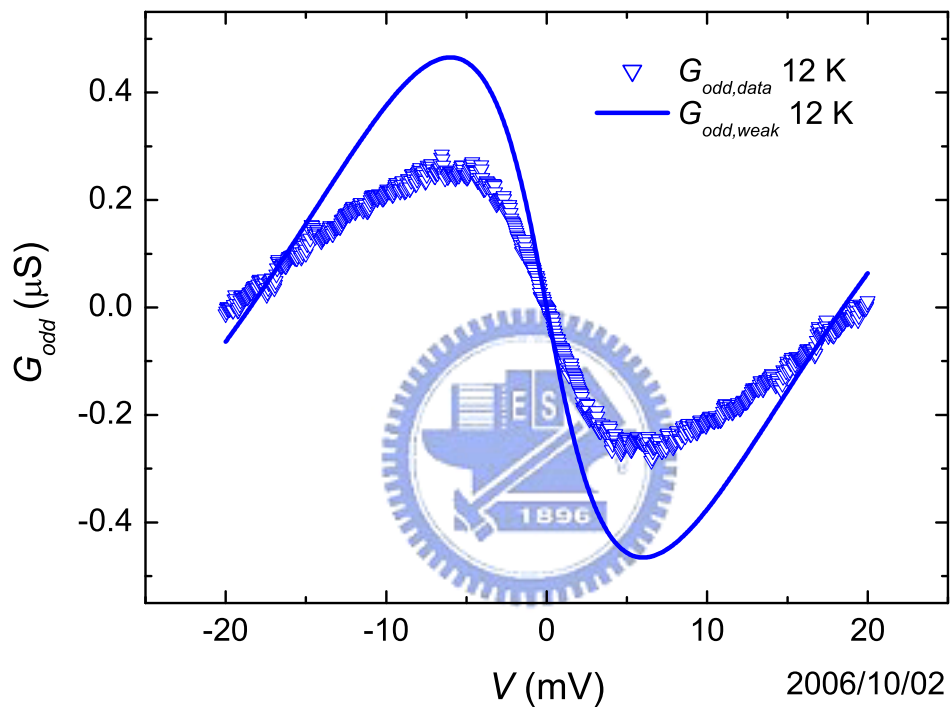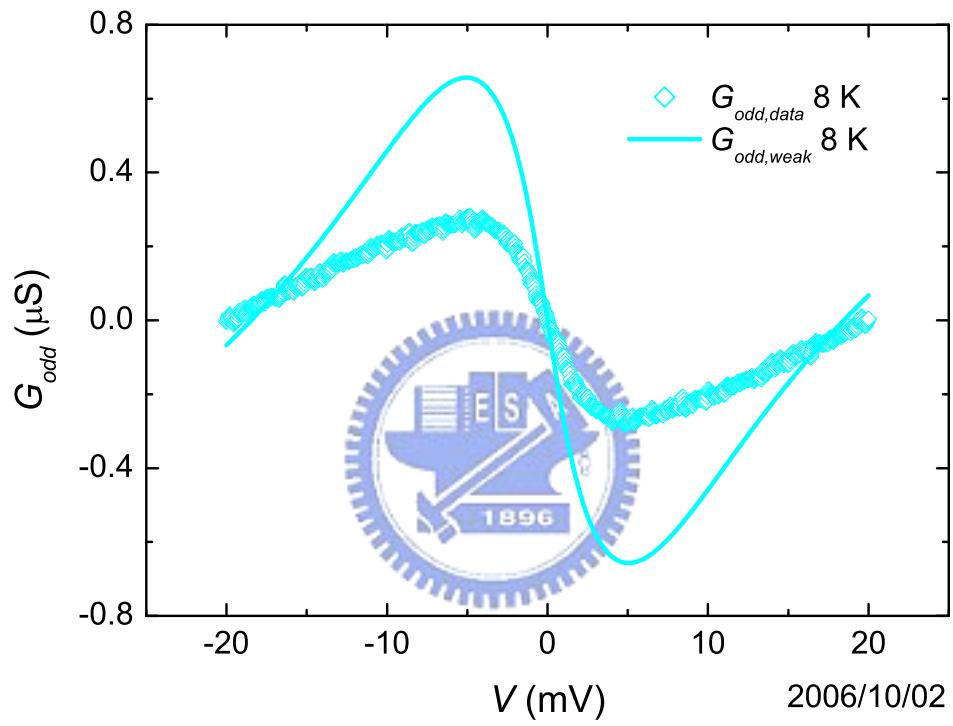Figure 4.35: The fitting of $G_{odd,data}(V,T)$ in terms of $G_{odd}^{weak}(V,T)$ at $T = 2.5$ K.

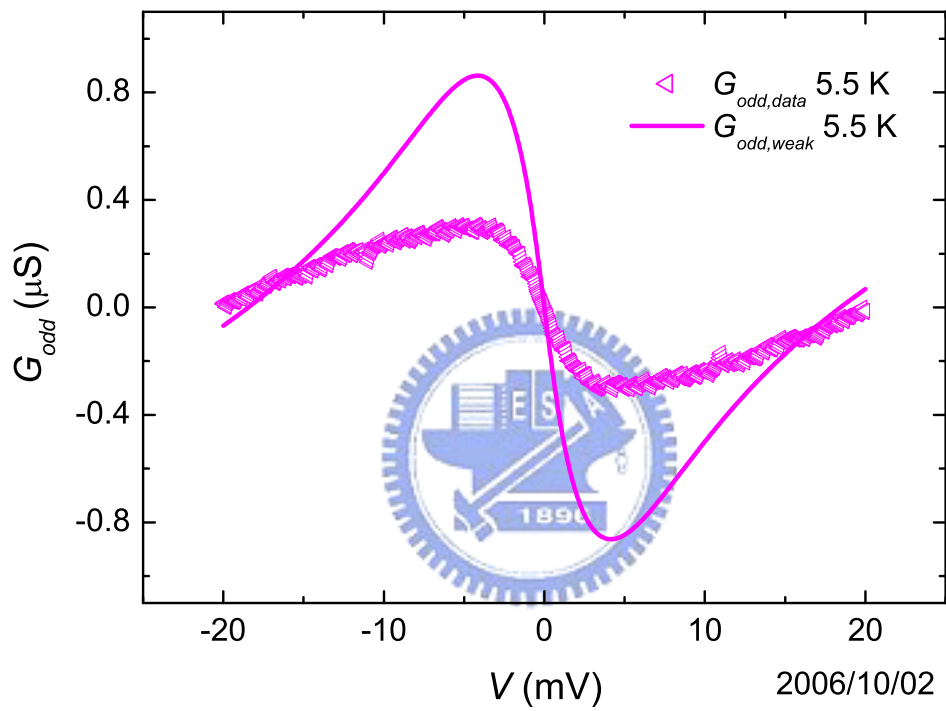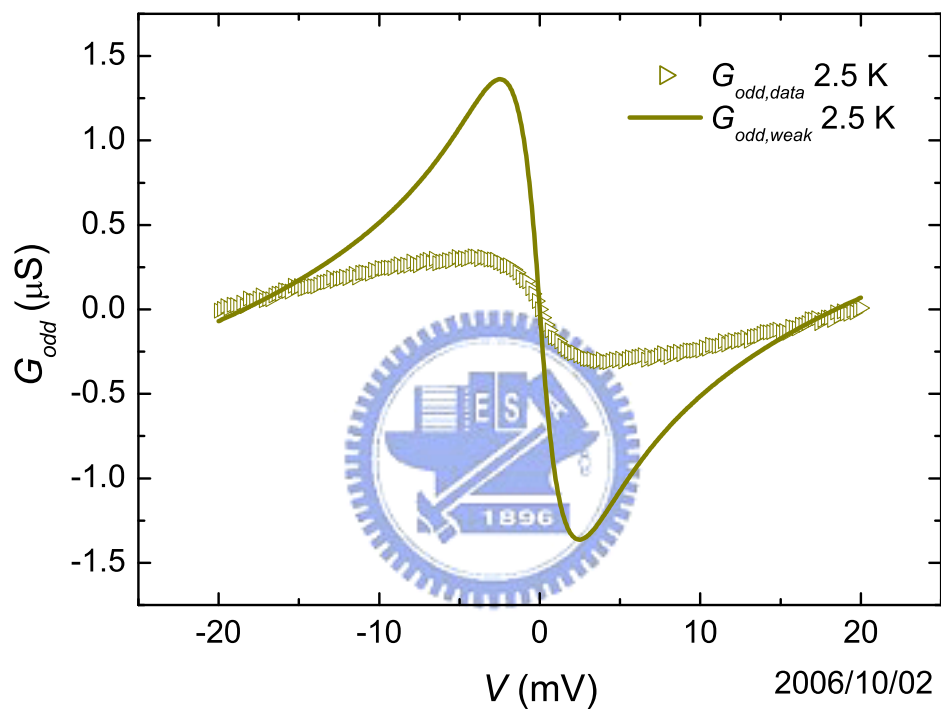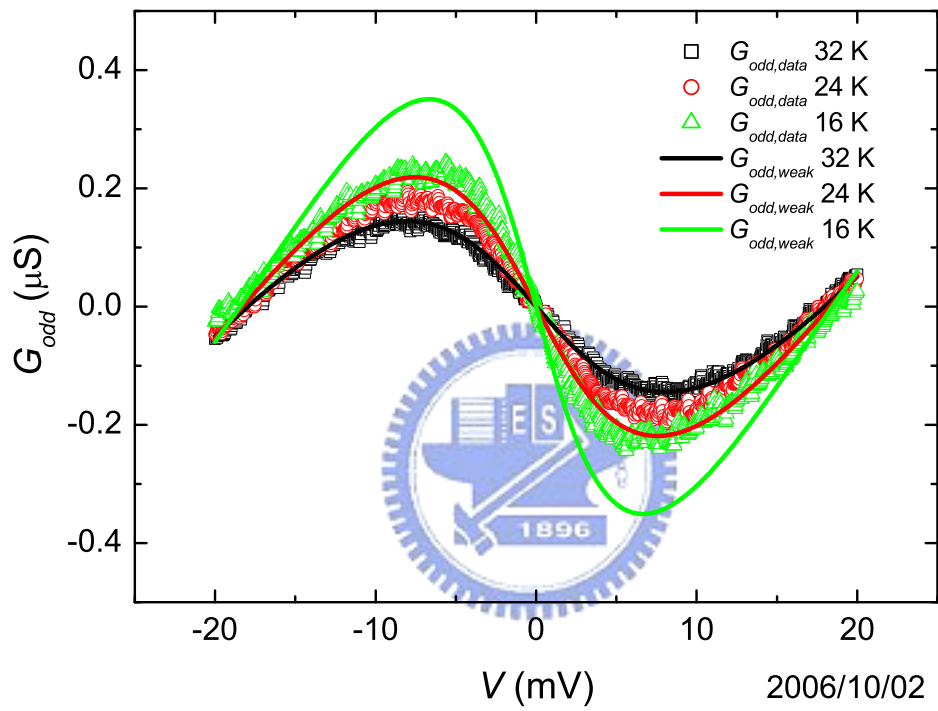Figure 4.36: The fitting of $G_{odd,data}(V,T)$ in terms of $G_{odd}^{weak}(V,T)$ at $T = 32$, 24, and 16 K.

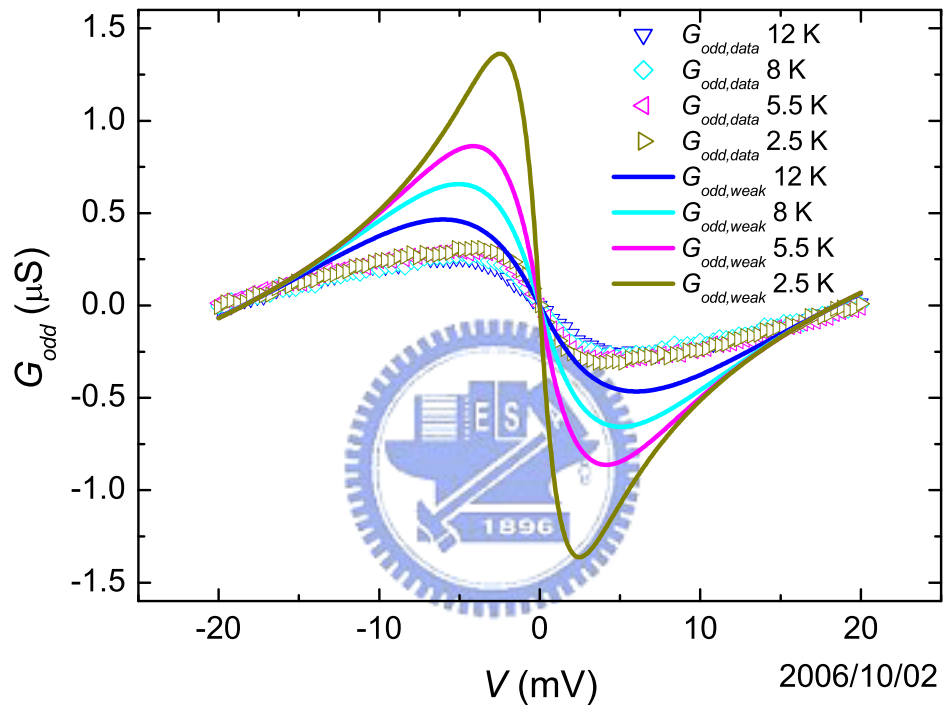Figure 4.37: The fitting of $G_{odd,data}(V, T)$ in terms of $G_{odd}^{weak}(V, T)$ at $T = 12, 8, 5.5,$ and 2.5 K.

Sample	$G_b(\mu\mathrm{S})$ at $\sim$ 50 K	A_j (mm^2)	G_b/A_j ($\mu\mathrm{S/mm}^2$)	T_K (K)	α
20060321	146.5	0.8	183.1	20.28	0.210 ± 0.010
20061002	82.5	0.5	165.0	38.03	0.207 ± 0.010
20061030	84.3	0.5	168.6	26.65	0.205 ± 0.010

Table 4.1: The fitted values of T_K and α in several Al/AlO$_x$/Sc tunnel junctions.

case, the resistance is replaced by conductance):

$$G_{NRG,empirical}(0,T) = G_0(0,0)(\frac{T_0^2}{T^2 + T_0^2})^\alpha, \tag{4.20}$$

where $T_0 = T_K/\sqrt{2^{1/\alpha} - 1}$, and $\alpha \approx 0.2 \pm 0.01$ for the $S = 1/2$ case. We fit the $G(0,T)$ data by (4.20) in several samples and show the fitting parameters in Table 4.1. The fitted values of T_K in different samples range from $\sim$ 20 K to $\sim$ 38 K, and the fitted values of α are all ~ 0.21 as shown in Table 4.1. This is consistent with the $S = 1/2$ case as we will expect in these Al/AlO$_x$/Sc tunnel junctions since the spin angular momentum of the diffused Sc atoms is $1/2$. We plot the data in these different samples, which was scaled using the corresponding parameters T_K and α, and the empirical expression (4.20) with $\alpha = 0.21$ together in Fig. 4.38. We find good agreement between the experimental data and the NRG calculations.

In addition to the reasonable value of α, we find the fitted values of T_K depend on the background conductance per unit junction area, G_b/A_j (A_j is the area of the junction cross section). The values of G_b/A_j and the corresponding fitted T_K in different samples are listed in Table 4.1. We find, in Table 4.1, the larger the G_b/A_j, the smaller the magnitude of T_K. On the other hand, we know the magnitude of G_b/A_j characterizes the thickness of the insulating barrier. The larger the G_b/A_j, the thinner the barrier and therefore, the larger the coupling strength Γ between
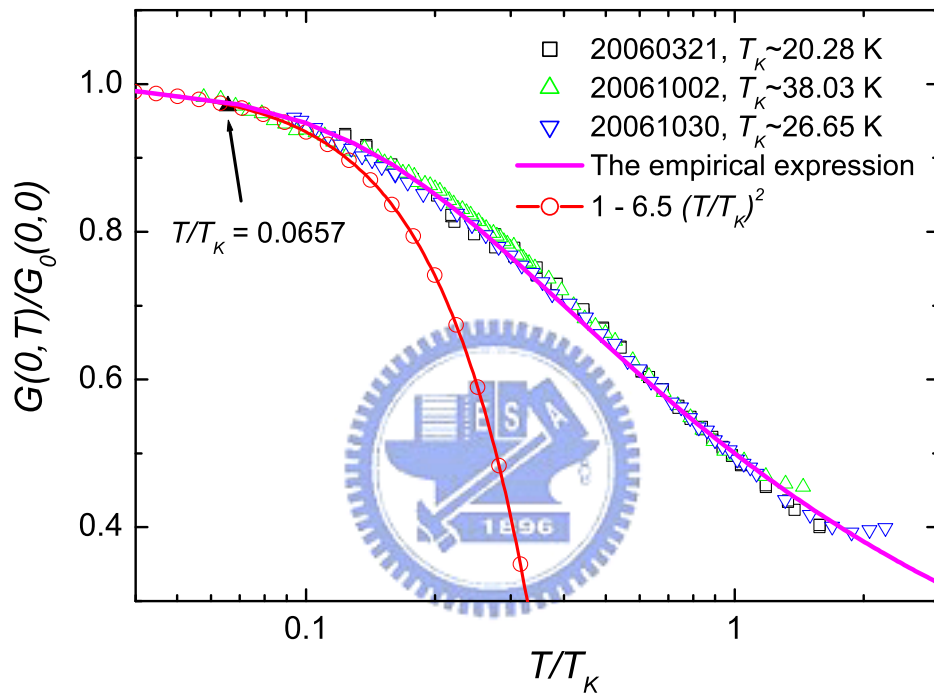
113

Figure 4.38: The fitting of $G_{even,data}(0,T)$ in terms of $G_{NRG}(0,T)$ for several Al/AlO$_x$/Sc tunnel junctions.

the free electrons and the localized states. According to [**?**, 21], T_K relates to Γ as

$$T_K = \frac{\Gamma}{2} e^{\pi \epsilon_0 (\epsilon_0 + U)/(\Gamma U)}, \tag{4.21}$$

From (4.21), the larger the Γ (the larger the G_b/A_j), the larger the T_K, which contracts to our results. The contradiction has also appeared in Lee *et al.*'s recent work [40], in which the Kondo effect in magnetic tunnel junctions was studied. They found T_K is larger in the longer oxidized (which will cause the thicker barrier and therefore the smaller Γ) samples.

Appelbaum [3] also calculated the dI/dV as a function of bias V in the strong coupling regime $(T \to 0)$, as mentioned in chapter 2. The even part of the conductance in the strong coupling regime, $G_{even}^{strong}(V)$, can be expressed as (see (2.155))

$$G_{even}^{strong}(V) = \frac{a_1 \times (eV)^2 + a_2 \times \Delta^2}{(eV)^2 + \Delta^2}, \tag{4.22}$$

where

$$a_1 = \frac{4\pi e^2}{\hbar} T_a^2 \rho^a(0) \rho^b(0),$$

$$a_2 = \frac{4e^2}{\hbar \pi (J\rho^a)^2} T_J^2 \rho^a(0) \rho^b(0),$$

$$\Delta = k_B T_K. \tag{4.23}$$

In Fig. 4.38, we find, for the sample "20061002", at 2.5 K $(T/T_K \approx 0.0657)$, the zero-bias conductance is passed through by a "$c - dT^2$" curve. This indicates that this sample is in in the strong coupling regime at 2.5 K. Therefore we can fit the $G_{even,data}(V, T = 2.5$ K$)$ in terms of (4.22). The fitting parameters $a_1 \approx 2.7$, $a_2 \approx 7$, and $\Delta \approx 3$ meV. This implies $T_K \approx 34.8$ K according to (4.23), and is quite consistent with the value (≈ 38 K) fitted by the empirical expression (4.20). The
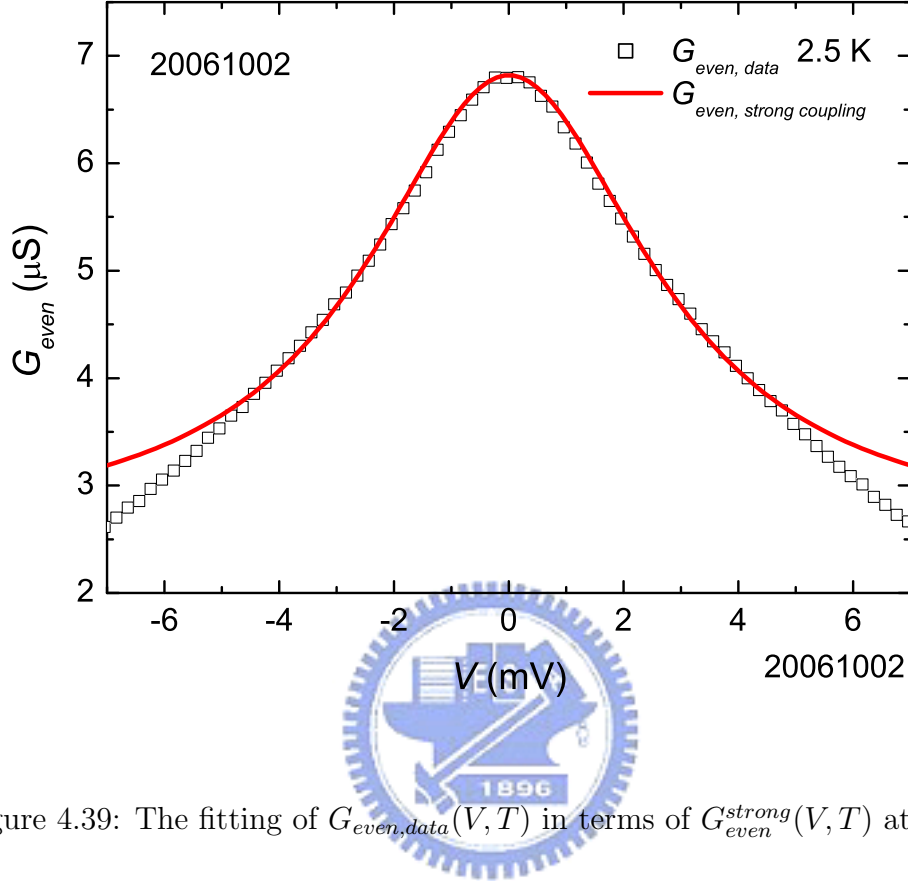
115

Figure 4.39: The fitting of $G_{even,data}(V,T)$ in terms of $G_{even}^{strong}(V,T)$ at $T = 2.5$ K.

results are shown in Fig. 4.39, and we find the theory (4.22) describes the data very well for -4 mV $\lesssim V \lesssim 4$ mV.

4.7   The Effect of Applying a Magnetic Field

So far we have analyzed the conductance spectra in both the weak and strong coupling regime, and fitted the zero-bias conductance for the whole temperature regime in terms of the NRG calculations. We attribute the phenomena we observed to the Kondo effect, i.e., the interaction between the tunneling electrons and the
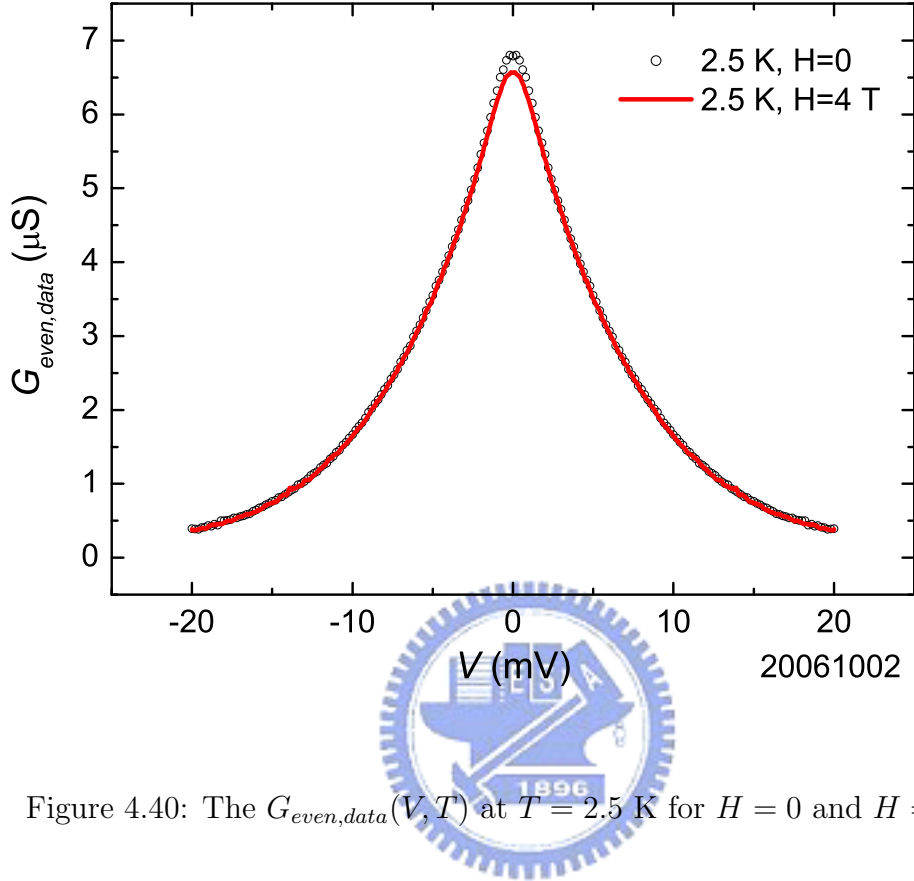
Figure 4.40: The $G_{even,data}(V,T)$ at $T = 2.5$ K for $H = 0$ and $H = 4$ T.

localized moments. There is a direct method to verify the existence of the localized moments: to apply a magnetic field H to the samples and see if the Zeeman splitting can be observed. We compare the conductance spectra for $H = 0$ and $H = 4$ T perpendicular to the junction cross section (parallel to the tunneling current) at 2.5 K in the "20061002" sample, and plot them in Fig. 4.40. We find there is no Zeeman splitting even under a magnetic field up to 4 T which can be shown in an enlarged plot Fig. 4.41. Theoretically, the splitting energy due to Zeeman effect $\Delta_{Zeeman} = g\mu_B H \approx 0.46$ meV (where we assume $g = 2$ in this case) is larger than the thermal smearing effect ≈ 0.22 meV at 2.5 K, and the splitting should
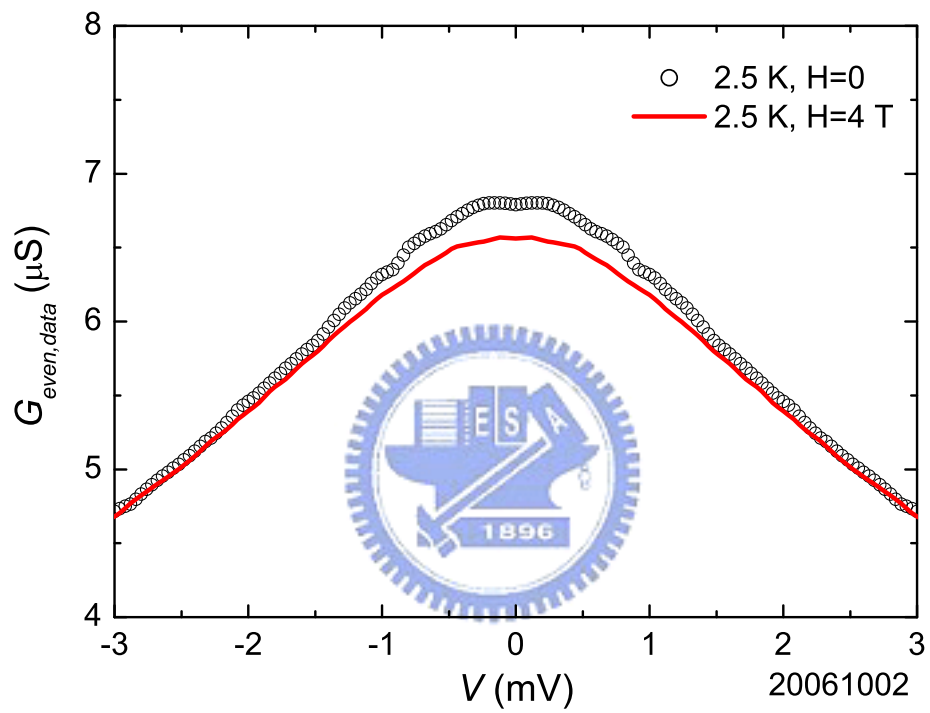
117

Figure 4.41: The $G_{even,data}(V, T)$ at $T = 2.5$ K for $H = 0$ and $H = 4$ T, which is enlarged from Fig. 4.40.

118

be observed. Indeed, the Zeeman splitting was widely observed in many literatures [41, 42, 43]. It seems a conflict to our assertion that the anomalies in the differential conductance are due to Kondo effect.

Recently, a theoretical work [33] indicated that there exists a critical magnetic field H_c above which the Zeeman splitting will occur. The value of H_c is dependent on temperature:

$$H_c \quad \approx \quad \frac{k_B T_K}{2g\mu_B}, \text{ for } 0 \leq T \leq \frac{T_K}{4} \qquad (4.24)$$

$$\approx \quad \frac{3k_B T}{g\mu_B}, \text{ for } T \geq \frac{T_K}{4} \qquad (4.25)$$

The Kondo temperature T_K in the "20061002" sample, according to the fitting of the $G_{even,data}(0,T)$ in terms of the NRG calculations, is ≈ 38 K. For $T = 2.5$ K, which is less than $T_K/4$ (≈ 9.5 K), $H_c \approx 14$ T according to (4.24). The magnetic field we applied, 4 T, is far below this critical value, and hence the Zeeman splitting was not observed.

4.8 Summary

In this chapter, we investigated Kondo effect in Al/AlO$_x$/Sc tunnel junctions by analyzing the zero-bias conductance as a function of temperature and the differential conductance dI/dV spectrum as a function of voltage at several temperatures. All the junctions had similar behaviors and we chose one, namely "20061002", to be discussed. Before the analysis proceeding, the quality of the insulating barrier was examined by measuring the superconducting gap of the Al film. The results demonstrated the leakage current through the barrier could be neglected and the conduction mechanism through the junction was *electron tunneling*. Besides, the

height and thickness of the AlO_x insulating layer in these $Al/AlO_x/Sc$ junctions can be determined by fitting the dI/dV spectra in $Al/AlO_x/Al$ junctions, whose barrier were grew with the same parameters as used to grow in the former, in terms of the BDR model. The fitting results showed reasonable values of the height and thickness.

After proving the good quality of the barrier, we turn to the dI/dV spectra in these $Al/AlO_x/Sc$ tunnel junctions. Although the dI/dV contained the contributions of the normal tunneling, of the $s-d$ exchange interaction, and of the DOS effect in the two metal leads, the last contribution was showed to be insignificant and could be neglected and the first contribution could be subtracted according to the BDR model. After the subtracting, the remainder conductance was found to contain an asymmetric term in it, and hence could be divided into an even term $G_{even,data}(V,T)$ and an odd term $G_{odd,data}(V,T)$.

$G_{even,data}(V,T)$ had a peak around zero-bias for $T \lesssim 32$ K, the lower the temperature, the higher the peak and the narrower the peak width. The zero-bias conductance $G_{even,data}(0,T)$ had a "$a - b\log T$" relation, namely the weak coupling regime, for 14 K $\lesssim T \lesssim 32$ K, and crossed over to a "$c - dT^2$" relation, namely strong coupling regime, for $T \lesssim 3.6$ K. In the weak coupling regime, both $G_{even,data}(V,T)$ spectra at several temperatures (32 K, 24 K, and 16 K) and $G_{even,data}(0,T)$ could be described by Appelbaum's perturbation theory, while outside the weak coupling regime, the perturbation calculation failed to describe the experimental data. In the strong coupling regime, we fitted the $G_{even,data}(V,T)$ spectrum at 2.5 K in terms of Appelbaum's self-consistent theory which was used to calculate in the strong coupling regime, and found a good agreement between the experimental data and the

theoretical calculation, and the Kondo temperature $T_K^{Appelbaum}$ could be extracted to ≈ 34.8 K from the fitting. On the other hand, we also fitted the $G_{even,data}(0,T)$ data in several samples in terms of the numerical renormalization group (NRG) calculation for the whole temperature regime (from weak to strong coupling regime), and the T_K^{NRG} could be determined from the fitting. In the sample "20061002", the fitted $T_K^{NRG} \approx 38$ K, and was quite consistent with the value of $T_K^{Appelbaum}$ (≈ 34.8 K). We attributed the existence of the $G_{odd,data}(V,T)$ to the effect of the interference between the $s-d$ exchange interaction enhanced tunneling and the impurity assisted tunneling, and tried to fit it by Appelbaum's corresponding calculation. We found the theory could describe the $G_{odd,data}(V,T)$ qualitatively, rather than quantitatively.

We also studied the effect of applying a magnetic field. For the sample "20061002" at 2.5 K, under the magnetic field 4 T, the zero-bias conductance decreased $\approx 3.4\%$ but no Zeeman splitting was observed. The absentation of the Zeeman splitting was due to the high T_K in this sample. A critical field $H_c \approx 14$ T, which was calculated using $T_K^{NRG} \approx 38$ K, was predicted to see the Zeeman splitting.